

1 **A Novel Method to Improve the Performance of PCM Thermal**  
2 **Energy Storage Units Using a Small Oscillator Plate-Numerical**  
3 **Analysis**

4  
5 S. Rahmanian<sup>1</sup>, H. Rahmanian-Koushkaki<sup>2</sup>, M. Moein-Jahromi<sup>1,\*</sup>, R. Saidur<sup>3,4,†</sup>

6  
7 <sup>1</sup> *Department of Mechanical Engineering, Engineering Faculty, Khalij Fars Avenue, Jahrom University, Jahrom,*  
8 *Iran, P.O. Box: 74135-111*

9 <sup>2</sup> *Department of Mechanical Engineering of Biosystems, Agriculture Faculty, Khalij Fars Avenue, Jahrom*  
10 *University, Jahrom, Iran, P.O. Box: 74135-111*

11 <sup>3</sup> *Research Centre for Nano-Materials and Energy Technology, School of Engineering and Technology, Sunway*  
12 *University, Jalan Universiti, Bandar Sunway, 47500 Petaling Jaya, Selangor, Malaysia*

13 <sup>4</sup> *School of Engineering, Lancaster University, Lancaster, LA1 4YW, UK*

---

**\*, † Corresponding authors:** M. Moein-Jahromi, R. Saidur

Email addresses: [s.rahmanian@jahromu.ac.ir](mailto:s.rahmanian@jahromu.ac.ir) (S. Rahmanian), [hrahmanian@jahromu.ac.ir](mailto:hrahmanian@jahromu.ac.ir) (H. Rahmanian-Koushkaki), [mmoein@jahromu.ac.ir](mailto:mmoein@jahromu.ac.ir) (M. Moein-Jahromi), [saidur@sunway.edu.my](mailto:saidur@sunway.edu.my) (R. Saidur).

## Abstract

Employing a small oscillator plate is proposed as a novel idea to improve the performance of phase change material (PCM) based thermal energy storage unit. This idea could make mixing heat flow toward the PCM solid-liquid interface to hasten the melting and heat transfer rates. Opposite to the vibration of the whole PCM heat sink suggested in the literature, it needs very slight mechanical energy for oscillation. The oscillator plate was installed at three positions for the horizontal and vertical PCM heat sink: i) the middle of the hot plate, ii) the bottom of the hot plate, and iii) the corner of the heat sink. A computational fluid dynamics model has been employed to model the PCM melting process and evaluate the induced mixing heat flow and its effect on natural convection. A new mechanical method using vibration energy accelerates heat flow to improve heat transfer and thermal energy absorption. The results reveal that in the best case with transversal oscillation at the corner of the heat sink, the melting rate and heat transfer rate (Nusselt number) increase by 39% and 64.2% compared to no vibration case, respectively. Also, the absorbed heat energy rate (AHR) within the PCM heat sink is elevated from 0.51 to 0.79 (54.9%), while the oscillator just consumed as small as 438 mJ of mechanical energy, reflecting this mechanical approach's uniqueness.

**Keywords:** Heat sink, Nusselt number, Oscillator, PCM, Thermal energy storage, Vibration.

## **1. Introduction**

Thermal energy storage (TES) technology has attracted increasing attention in recent years. This technology has demonstrated its advantages in two main fields: thermal management and renewable energy, especially solar systems. The time and intensity mismatch between solar energy supply and energy demand can be addressed by integrating TES with solar systems. TES can also be applied effectively in cooling electronic devices, battery thermal management, waste heat recovery, energy harvesting, building heating/cooling, and other potential applications. Storing thermal energy can be performed via sensible heat or latent heat storage, depending on the operation condition and working fluid. However, latent heat storages possess higher storing potential and, as a result, reduce the requisite volume of material for designing a compact system for a specific quantity of thermal energy [1].

Phase change materials (PCM) are substances whose phase change is exploited in engineering and industrial processes. Phase transformation between solid and liquid is the most common state for PCM that absorb and release latent heat with orders of magnitude higher than the sensible heat [2]. Owing to the low cost and long life of common PCM, thermal management has been developed by including PCM to control the temperature fluctuation of electronic devices. Alternating power loads usually cause hot spots in photovoltaic modules, chips, or batteries. PCM has emerged as a superior method to overcome this challenge for developing high-performance electronic apparatuses. The priority of PCM in the TES system originates from its narrow operating temperature for the melting/solidification process. Therefore, it can store high thermal energy at a small temperature interval, preventing high-temperature thermal issues.

In contrast to the high latent heat of PCM, their inferior thermal conductivity diminishes the heat transfer rate during the melting or solidification of PCM. Therefore, thermal energy storage or extraction rate would be limited significantly. It is considered an extensive challenge for

applications comprised of high power rates or severe oscillation of thermal charging/discharging. Thermal conduction regulates the heat transfer in the solid phase, whereas natural convection governs the dominant thermal process in the liquid phase of PCM. Such shortcoming in PCM thermophysical property has provided a wide research field to improve thermal conductivity or natural convection in PCM. With less attention to convection, most research has been devoted to modified thermal conduction by various methods, such as the incorporation of metal fin [3,4], metal or carbon foam [5,6], or nanoparticles in PCM [7].

Inserting the fin in the PCM enclosure has been introduced as the first attempt to boost heat transfer with low cost and simple technology by extending the surface. Eslami et al. [8] reviewed the effect of fin parameters such as fin number, dimension, position as well as fluid properties on the performance of TES. Zhang et al. [9] proposed that helical fins and topology optimization could offer exceeding performance, while this enhancement is also limited and requires additional techniques beyond fin.

Dispersion of nanoparticles with high thermal conductivity has been confirmed as an impressive method to modify the thermophysical properties of PCM, even at very low volume fractions [10]. Li et al. [11] used graphite nanosheets and silver nanoparticles to modify the thermal conductivity of polyethylene glycol from 0.26 to 3.1  $\text{W}\cdot\text{m}^{-1}\cdot\text{K}^{-1}$  at the cost of 13% reduction of latent heat. Nie et al. [12] demonstrated the effect of nanoparticle-PCM with a gradient pattern in shell-tube latent heat storage (LHS) through numerical simulation. In another research by Kittusamy et al. [13], enhancing thermal conductivity of nanocomposite-PCM was reported along with 6 times enhancement of dynamic viscosity at 70 °C. According to the literature, there is an upper limit for nanoparticle concentration in PCM and, consequently, a bound for conductivity intensification. In addition, nanoparticle dispersion and nanofluid stability are a concern in this material category.

Utilizing metal or carbon foam as porous media in PCM emerged as a recent attempt to accelerate the melting/solidification of PCM by improving effective thermal conductivity for composite PCM/foam. Pore density, porosity, and other foam geometrical factors determine the composite's overall conductivity [14]. A copper foam with 92% porosity could increase the thermal conductivity of RT35 from 0.2 to 8.76 W .m<sup>-1</sup>.K<sup>-1</sup> besides around 50% reduction of latent heat [15]. From another point of view, porous foam media declines the natural convection and temperature difference in the PCM-composite, and it has impressive performance for transferring the heat to a far location from the heat source[16].

In addition to the separate employment of these techniques, the combination of nanoparticle-fin [17], nanoparticle-foam [18], and fin-foam [19] have been investigated, too. The synergic effects of these methods usually improve the heat transfer and thermal performance of the PCM system. However, these declared methods' disadvantages are increasing the weight, cost, and dynamic viscosity and decreasing the latent heat and natural convection. Therefore, other approaches, such as applying a magnetic field, ultrasonic wave, and low/high-frequency vibration, have been explored more recently [20].

Ultrasonic vibration was demonstrated in some experimental research to improve the melting and solidification of PCMs [21]. The power and action time of ultrasonic vibration effectively reduced the melting time of a eutectic mixture by creating a streaming effect as a turbulence effect [22]. Compared to the natural melting, cavitation, and fluctuating fluid motion were also distinguished as compelling factors by applying ultrasonic to accelerate the heat storage up to 2.5 times. In addition, mechanical vibration has also been applied to the PCM system to improve heat transfer. In experimental work, battery thermal management was conducted under mechanical vibration with a 10-30 Hz frequency and 2-4 mm amplitude. Small amplitude and moderate frequency were proven as optimum conditions to prolong the operating time of composite-PCM

[23]. Numerical simulation reported similar results indicating an upper amplitude limit for improving heat transfer [24]. Besides vibration frequency and amplitude, the orientation of the vibration axis was examined as a variable for a square enclosure of PCM by implementing the Lattice-Boltzmann approach [25,26]. The obtained results revealed the noteworthy effect of vibration angle, especially under low frequency, with faster response in vibrating parallel to gravity. All the presented research about the mechanical vibration improvement approach suggested a volumetric vibration of the whole PCM container associated with an oscillating gravitational acceleration. Considerable mechanical energy is required for the volumetric oscillation. So, in this paper, a small oscillator plate is proposed to be installed at different positions to enhance the heat transfer rate as same as the oscillation of the whole PCM container with deficient mechanical energy consumption. It is a novel idea to reduce the drawbacks of whole volumetric vibration in previous papers.

It is evident from the preceding literature review that there are few studies on the impact of mechanical vibrations on the PCM charging process. Through numerical simulations, this work aims to fill this knowledge gap. Low-frequency mechanical vibrations generated unintentionally or indirectly are common in most manufacturing areas. Therefore, low-frequency vibration can be exploited to improve heat absorption of the PCM storage system. In all previous papers [27], the whole PCM enclosure experienced mechanical vibration by defining a moving boundary condition or applying an additional gravity acceleration vector. However, considering the mass of the PCM enclosure, significant mechanical or electrical energy is required to generate the desired vibration, which may not be cost-benefit. For the first time, a new vibration mechanism is introduced in the current study to accelerate the charging process of latent heat storage (LHS) LHS system with very little energy consumption. In this novel system, there is the capability of controlling the vibration amplitude and frequency to manage heat transfer. A numerical simulation was performed to

evaluate the potential of this novel mechanism for an LHS system in two different situations, vertically and horizontally. A small oscillator plate is installed on the inner wall of a PCM enclosure but in three different positions to examine the effects of location on natural convection. Different vibration amplitude was also applied to the oscillator under low frequency to find the optimum operating conditions. The charging processes of this LHS system, including melting rate, liquid fraction, mean temperature of PCM, convective heat transfer rate (Nusselt number), and stored heat energy, were presented. The remaining parts of the paper are arranged as follows: The numerical model description, including the governing equations for phase change material melting processes and the boundary conditions, model input parameters, investigated domain, and solution procedures, are discussed in Section 2. Section 3 contains a list of the numerical methods, followed by the numerical validation and discussion. Section 4 includes the main concluding remarks. The effect of this novel oscillator on the PCM charging process is then concluded.

## **2. Model Descriptions**

The main points of the numerical model of a rectangular PCM-based TES shown in Fig. 1 have been described during the phase-changing process. Fig. 1 schematically shows a rectangular thermal energy storage unit in two horizontal and vertical orientations with a small oscillator plate in three different positions, forming the six cases studied in this paper. The width and length of the enclosure are 30 mm and 60 mm, respectively. As indicated in Fig. 1, an oscillator plate with a length of 5 mm is used in each enclosure to study the effect of a small mechanical vibration system on improving the heat transfer mechanism and the heat stored in TES during the charging process. However, three different places of the oscillator are also suggested to check the effect of its location and find the optimum case. In all cases, a thin plate was assumed as an oscillator located near the heat source with two specific positions at the middle and corner of the hot plate. The vibration direction of the oscillator is parallel to the enclosure wall in all situations. RT-35, a

standard PCM, is considered the phase change material in the current research. Thermo-physical properties of RT-35 are reported in Table 1.

## 2.1. Assumptions

The main significant assumptions considered in the modeling process are as follows:

- (a) The model is two-dimensional.
- (b) The flow of the liquid zone is assumed to be incompressible, Newtonian, and transient for all cases.
- (c) The Boussinesq model represents the density changes and their effect on natural convection.
- (d) The changes in thermo-physical properties of the PCM in the mushy zone are considered continuous and linearly by the volume fraction.
- (e) The viscous-dissipation term is negligible.

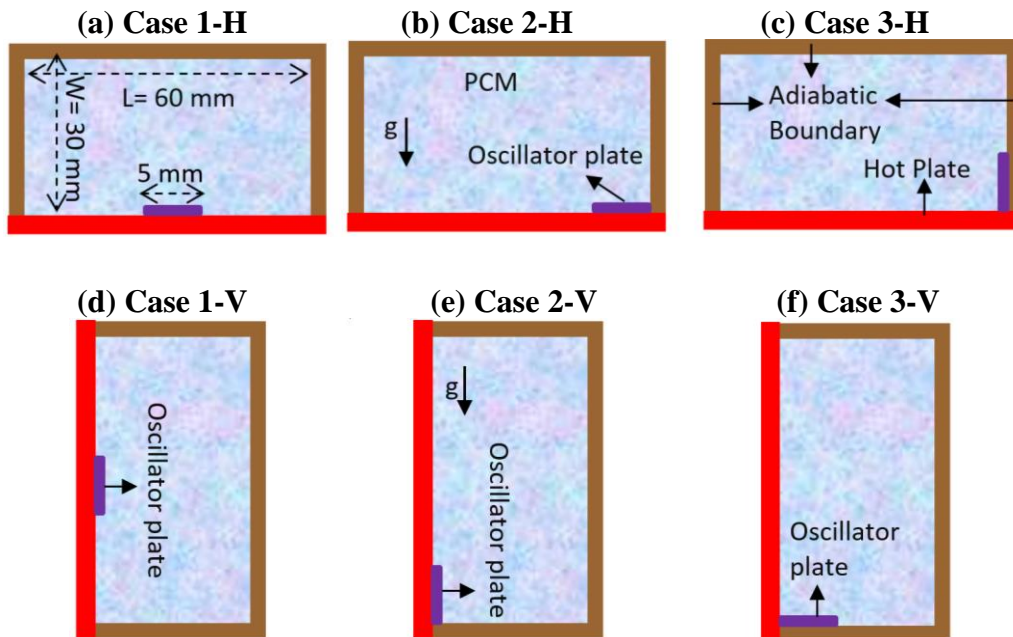


**Fig. 1.** Schematic view of the thermal energy storage units equipped with an oscillator plate, (a) to (c) are horizontally oriented, and (d) to (f) are vertically oriented PCM containers.

## 2.2. Governing equations

The enthalpy-porosity method was applied to model solid-liquid phase changing during TES charging [28]. In addition, the conservation equations, including the continuity, momentum, and energy, are used as [29]:

**Continuity equation:**

$$\frac{\partial \rho_{pcm}}{\partial t} + (\vec{\nabla} \cdot \rho_{pcm} \vec{V}) = 0 \quad (1)$$

**Momentum equation in x-direction:**

$$\rho_{pcm} \left[ \frac{\partial u}{\partial t} + (\vec{V} \cdot \vec{\nabla}) u \right] = \frac{-\partial P}{\partial x} + \mu_{pcm} \nabla^2 u - \rho_{pcm} \beta_{pcm} g_x (T_{pcm} - T_0) + S_{x,pcm} \quad (2)$$

**Momentum equation in y-direction:**

$$\rho_{pcm} \left[ \frac{\partial v}{\partial t} + (\vec{V} \cdot \vec{\nabla}) v \right] = \frac{-\partial P}{\partial y} + \mu_{pcm} \nabla^2 v - \rho_{pcm} \beta_{pcm} g_y (T_{pcm} - T_0) + S_{y,pcm} \quad (3)$$

In the above equations,  $\vec{V}$ ,  $u$ ,  $v$ ,  $\rho$ ,  $\mu$ ,  $\beta$ ,  $g$ , and  $T$  are the velocity vector, x-component of the velocity vector, y-component of the velocity vector, density, viscosity, thermal expansion coefficient, gravitational acceleration, temperature.  $S_{x,pcm}$ , and  $S_{y,pcm}$  are the x-component and y-component of the momentum source term, respectively, which are used for velocity damping in the solid phase of the PCM [5]. They are defined as:

$$S_{x,pcm} = A_{mushy} \frac{-(1 - L_f)^2}{L_f^3 + \epsilon} u \quad (4)$$

$$S_{y,pcm} = A_{mushy} \frac{-(1 - L_f)^2}{L_f^3 + \epsilon} v \quad (5)$$

In the last two equations,  $A_{mushy}$  is the mushy zone constant,  $\epsilon = 0.001$  is a small number to avoid division by zero and  $L_f$  is the liquid fraction varies between zero for the solid phase to one for the liquid phase and which is calculated as:

$$L_f = \frac{T_{pcm} - T_s}{T_l - T_s} \quad (6)$$

where  $T_s$  and  $T_l$  are solidus and liquidus temperatures of the PCM, respectively.

### Energy equation:

$$(\rho C_p)_{pcm} \left[ \frac{\partial T_{pcm}}{\partial t} + (\vec{V} \cdot \nabla T_{pcm}) \right] + \rho_{PCM} \frac{\partial H_{PCM}}{\partial t} = \nabla \cdot (k_{pcm} \nabla T_{PCM}) \quad (7)$$

where  $C_p$  and  $k$  are the specific heat capacity and thermal conductivity of the PCM, respectively [30].

$H_{PCM}$  is the PCM total enthalpy computed by summation of the sensible and latent heat as follows:

$$H_{PCM} = \underbrace{h_{ref} + \int_{T_{ref}}^T (C_p)_{PCM} dT}_{sensible} + \underbrace{L_f}_{latent} h_{sl} \quad (8)$$

$h_{sl}$  in Eq. (8) reflects the latent heat of fusion for the PCM

### 2.3. Boundary and initial conditions

As shown in Fig. 1, the boundary conditions are expressed as follows:

- The momentum boundary conditions are considered no-slip for all the walls with zero velocity except the oscillator plate.
- For the oscillator plate, the velocity is set as a translational moving wall,  $V_p$ , such as:

$$V_p = V_a \sin(2\pi f \cdot t) \quad (9)$$

where,  $V_a$  and  $f$  are the amplitude and frequency of the oscillating velocity function. As the base case,  $V_a$  is set to  $0.01\pi$  ( $m s^{-1}$ ) and  $f$  is set to 10Hz.

- The thermal boundary conditions are chosen adiabatic with zero heat flux for all brown walls in Fig. 1.
- For the red wall in Fig. 1, the thermal boundary condition is considered isothermal ( $T_H = 70^\circ C$ ).

It is worthwhile to mention that the temperature of the PCM is considered  $T_0 = 27^\circ C$  for the initial condition.

## 2.4. Thermo-physical parameters

The thermophysical properties of the PCM (RT35) in both solid and liquid phases are given in Table 1.

**Table 1.** Thermo-physical properties of materials used in this study [31] and for validation [34].

Properties	Symbol (unit)	Solid at $T_s = 29$ °C)	Liquid at $T_l = 36$ °C)	Validation case ( $T_l = 30$ °C)
Density	$\rho$ ( $kg m^{-3}$ )	860	770	800
Latent heat of fusion	$h_{sl}$ ( $J kg^{-1}$ )	160000		125000
specific heat capacity	$C_p$ ( $J Kg^{-1}K^{-1}$ )	2000	2000	1250
Thermal conductivity	$k$ ( $W m^{-1}K^{-1}$ )	0.2	0.2	0.2
Thermal expansion coefficient	$\beta$ ( $K^{-1}$ )	-	0.0006	0.002
Viscosity	$\mu$ (Pa s)	-	0.023	0.008
Thermal diffusivity	$\alpha$ ( $m^2 s^{-1}$ )	-	$1.3 \times 10^{-7}$	$2 \times 10^{-7}$

## 2.5. Post-processing equation

For post-processing purposes, three quantities have been defined in this section. The first is the heat transfer rate in the form of the Nusselt number of the heat sink, the second is the total mechanical energy required for the oscillator plate, and the third is the **absorbed heat energy rate** in each case. They are described in the following:

a) Nusselt number

The Nusselt number is defined as follows [32]:

$$Nu = \frac{h W}{K_{PCM}} \quad (10)$$

In which  $h$ ,  $W$  and  $K_{PCM}$  are the heat transfer coefficient, the width of the PCM thermal energy storage unit, and the PCM thermal conductivity, respectively. The heat transfer coefficient,  $h$ , is obtained from:

$$h = \frac{q_s''}{T_s - T_L} \quad (11)$$

where,  $q_s''$  is the heat flux which enters the PCM heat sink from the hot plate,  $T_s$  is the hot plate temperature, and  $T_L$  is the PCM liquidus melting temperature.

b) The total mechanical energy of the oscillator

The total mechanical energy of the oscillator is computed by integration from the power of drag force over the complete melting time, so it is:

$$E_{mech} = \frac{W^2}{\alpha} \int_0^{Fo_f} P_d dFo \quad (12)$$

Where  $Fo$  is Fourier number stands as dimensionless time, it is defined as  $Fo = \alpha t/W^2$ .  $\alpha$  is thermal diffusivity which is reported in Table 1.  $Fo_f$  denotes the dimensionless complete melting time, and  $P_d$  is the mechanical power which is needed to overcome the friction drag force, which is calculated as:

$$P_d = - \underbrace{\int_0^{L_p} (\tau_w dA)}_{F_d} \times V_p \quad (13)$$

Where  $F_d$  is the drag force which is computed by integrating from the wall shear stress ( $\tau_w$ ) on the surface of the oscillator plate ( $dA$ ).  $V_p$  is the vibration velocity function of the oscillator plate described in Eq. (9). For more explanation, the plate was assumed with thin thickness; therefore, only the drag force is applied on the plate surface. For calculating the required power for oscillator vibration, the force is multiplied by plate velocity. The drag force originated from the shear stress applied on the plate surface non-constantly, and it should be integrated on the whole surface.

### c) Absorbed heat energy rate (AHR)

The total absorbed heat energy is computed by time integration from the heat flux that enters the thermal energy storage unit from the hot plate. It is [32]:

$$E_{heat}(Fo) = \frac{W^2}{\alpha} \int_0^{Fo_f} q_s'' (D \times L) dFo \quad (14)$$

Where  $D$  and  $L$  are the depth and length of the PCM heat sink, respectively.

The net absorbed heat energy could be obtained by subtracting the equivalent energy which is required for the oscillator plate as follows [33]:

$$E_{heat,net}(Fo) = E_{heat}(Fo) - \frac{E_{mech}(Fo)}{\eta_{elec}} \quad (15)$$

Where,  $E_{mech}$  is the total mechanical energy of the oscillator plate as described in Eq. (12), and  $\eta_{elec}$  is the prevalent efficiency of conventional power plants. Finally, the absorbed heat energy rate,  $AHR( Fo )$ , could be defined as the ratio of net absorbed heat energy up to desired dimensionless time ( $Fo$ ),  $E_{heat,net}( Fo )$ , to total energy which the PCM thermal energy storage unit can store from the initial state to reach to final temperature, say  $T = T_H$ ,  $E_{heat,total}$ , so one can say:

$$AHR( Fo ) = \frac{E_{heat,net}( Fo )}{E_{heat,total}} = \frac{E_{heat,net}( Fo )}{m_{PCM}C_{P,PCM}(T_l - T_0) + m_{PCM}h_{sl} + m_{PCM}C_{P,PCM}(T_H - T_l)} \quad (16)$$

In which,  $m_{PCM}$ ,  $C_{P,PCM}$ ,  $h_{sl}$ ,  $T_0$ , and  $T_l$  are mass, heat capacity, latent heat of fusion, initial temperature liquidus temperature of PCM, respectively.  $T_H$  is also the hot wall temperature which is considered the final PCM temperature. It is worth noting that according to the dimension of the thermal storage heat unit, PCM properties, and boundary condition, the total energy which the PCM heat sink can store is computed as  $E_{heat,total} = 22.66$  kJ, in this paper.

## 2.6. Solution procedures

All suggested thermal energy storage units have been simulated by solving the governing equations according to the boundary conditions based on the Finite Volume Method (FVM) in the Ansys Fluent 2020R2 software package. The system of continuity and momentum equations, Eqs. (1)-(3) are solved using the semi-implicit method for the pressure-linked equations (SIMPLE) algorithm to handle the velocity-pressure coupling. The solution domains are discretized using a quadratic mesh grid with satisfactory refinement and smoothness to predict the required parameters with a high gradient. On the other hand, the governing equations are discretized using a second-order central difference upwind scheme over the cells to diminish the dispersion errors and increase the accuracy, especially for nonlinear convection and diffusion terms. However, a

grid size study is also performed considering three distinctive grid sizes: coarse, medium, and fine, to ensure the independence of the solution with respect to the grid size. Also, an independency study of time step size is accomplished with three different time steps of 0.025 s, 0.02 s, and 0.01 s. The convergence criteria are considered at low residuals of less than  $10^{-4}$  at each time step. For example, the medium mesh grid of Case 1-H is shown in Fig. 2. After the mesh grid and time step study; the remaining post-processing is conducted based on the optimum mesh grid and time step sizes.

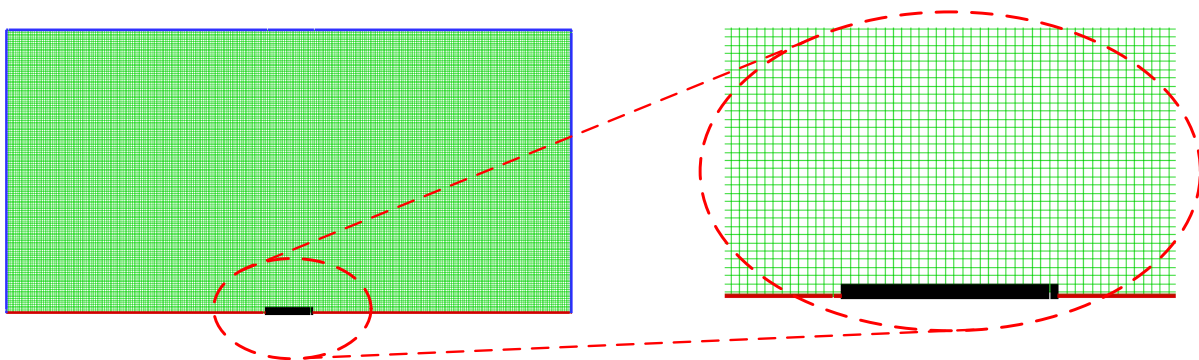


**Fig. 2.** Sample of solution domain with the mesh grids for Case 1-H. Red line: hot plate, blue lines: adiabatic boundaries, black line: oscillator plate.

## 2.7. Validation and mesh study

At first, the model has been validated against the published data in the literature [34]. Secondly, the independency of the simulation concerning grid size and time step has been evaluated.

Due to the lack of research about PCM-based thermal energy storage units equipped with a small oscillator plate, for validation purposes, a complete computational fluid dynamics (CFD) model has been employed to simulate a cubic PCM-based thermal storage unit with whole volumetric vibration which was modeled using the Lattice Boltzmann method by Wu et al. [34].

The volumetric vibration of the whole PCM volume has been modeled in the current CFD

simulation by using a periodic time function of gravity. So, in order to simulate the whole volumetric vibration, a fluctuating gravity function is substituted with the gravity components  $g_y$  in momentum equations Eq. (3); it is considered as [25]:

$$g_y = -g \left[ 1 + \frac{b \times \left( \frac{fL^2}{\alpha} \right)^2}{g} \sin \left( \frac{fL^2}{\alpha} t \right) \right] \times \cos(\theta) \quad (17)$$

Where  $g$  is gravity in the  $y$ -direction,  $b$  is the amplitude of gravity fluctuation,  $f$  is vibration frequency,  $\alpha$  is PCM thermal diffusivity,  $L$  is the cubic length, and  $\theta$  is the angle between vibration direction and the gravity vector, here it is zero for the validation case. Considering this fluctuating gravity function could simulate the physics of volumetric vibration of the PCM heat storage unit. Meanwhile, to simulate the same situation of Ref. [34], the no-slip condition ( $u, v = 0$ ) is applied on all walls of the cubic PCM-based thermal storage unit, while the adiabatic condition is considered for three of the walls and constant temperature condition is applied for the fourth wall (hot wall,  $T = T_H$ ). All geometrical, thermophysical, structural, and operating parameters have been considered for validation, as mentioned in [34]. In this regard, some of the thermophysical properties of the PCM used for validation purpose is expressed in Table 1. Also, the cubic length is  $L = 0.1$  m, and the initial temperature is  $T_0 = 300$  K. It should be noted that the temperature of the hot wall  $T_H$  and the amplitude of gravity fluctuation,  $b$ , could be determined when the Rayleigh number ( $Ra = (g\beta(T_H - T_0)L^3)/(\alpha\nu)$ ) and Grashof number ( $Gr = (\beta bf(T_H - T_0)L^2)/(2\nu^2)$ ) are considered as  $10^4$  and  $10^6$ , respectively [34]. The validation results have been shown in Fig. 3 for the liquid fraction and Nusselt number versus dimensionless time (Fourier number) at a low vibration frequency of 0.0002 Hz. As shown in Fig. 3, the present simulation could predict the trend of time profiles for the liquid fraction and Nusselt number very well. The present CFD model coincides with the Lattice Boltzmann model by Wu et al. [34], especially for  $Fo < 0.3$ , in which

the conductive heat transfer is dominant. However, the variations in liquid fraction and Nusselt number are also anticipated with a very good agreement with Wu et al.'s models.

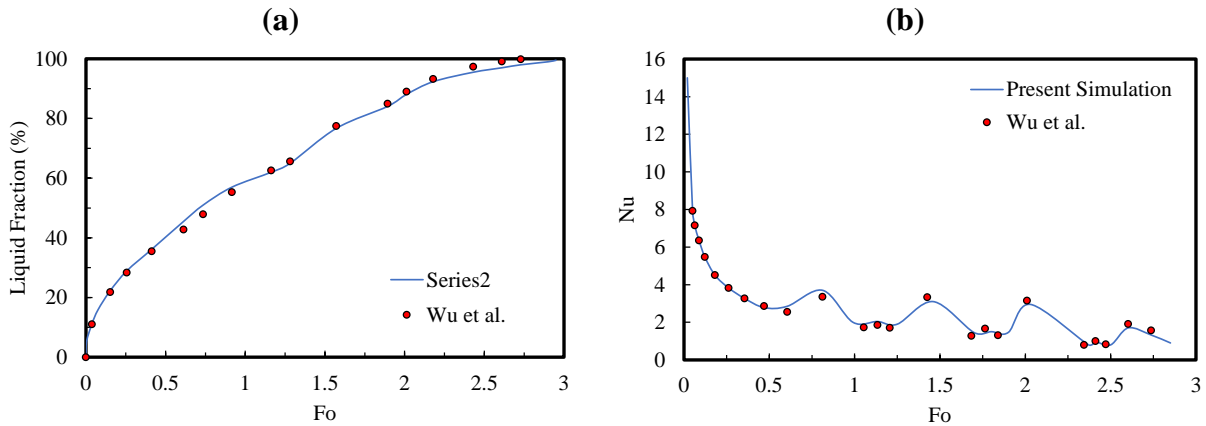


**Fig. 3.** Validation of the present simulation against the numerical modeling of Wu et al. [34], (a) liquid fraction, and (b) Nusselt number for frequency of 0.0002 Hz.

To ensure the independence of the solution with respect to the grid size and time step size, the solution's output has been computed and compared for three different mesh grid sizes and time steps. Fig. 4 shows the independence of the time profile of liquid fraction as the most important solution output with respect to grid size and time step for Case 3-H, as an example. Three mesh grid sizes, including a coarse grid with 27,400 cells, a medium grid with 46,310 cells, and a fine grid with 78,300 cells, have been studied and compared here. As indicated in Fig. 4(a), the solution results are close to each other for these three grid sizes, especially since there are very few changes between the medium and fine grids. On the other hand, three time-steps, 0.025, 0.02, and 0.01 s, are considered to investigate the solution time step independence. According to Fig. 4(b), all three time-steps yield similar time profiles for the liquid fraction. As a result, one can say that the present CFD model is independent of the mesh grid size and the time step size.

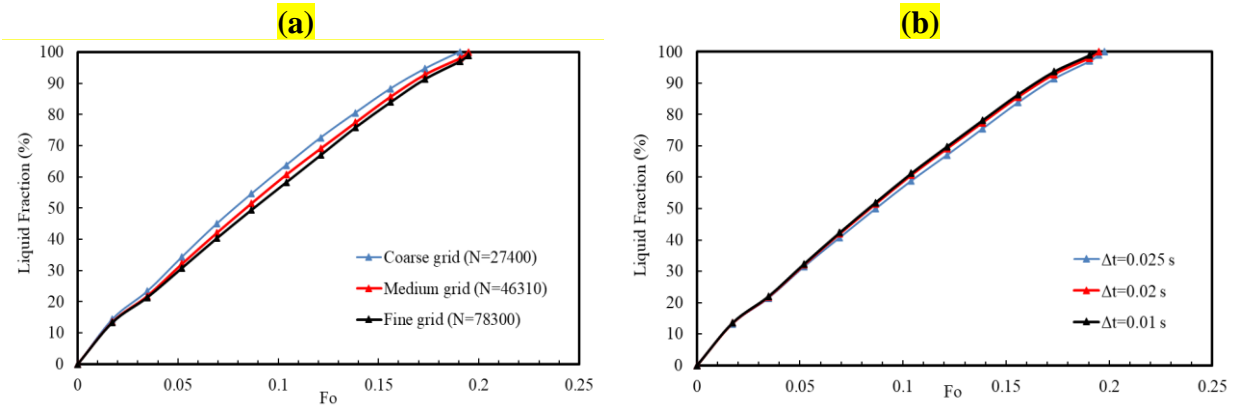


**Fig. 4.** Solution independency study with respect to (a) grid size and (b) time step for Case 3-H.

### 3. Results and Discussions

The results of the numerical model of a PCM-based thermal energy storage unit equipped with a small oscillator plate have been presented in this section. The main significant results of current modeling have been expressed in the following sections.

The results of the current simulation will be described, compared, and discussed for all the horizontally- and vertically-oriented thermal energy storage units equipped with small oscillator plates, which already have been presented in Fig. 1.

The performance of the three horizontal thermal energy storage units, including Cases 1-H, 2-H, and 3-H, are expressed in Fig. 5 and compared with a horizontal thermal storage unit without an oscillator (Control-H).

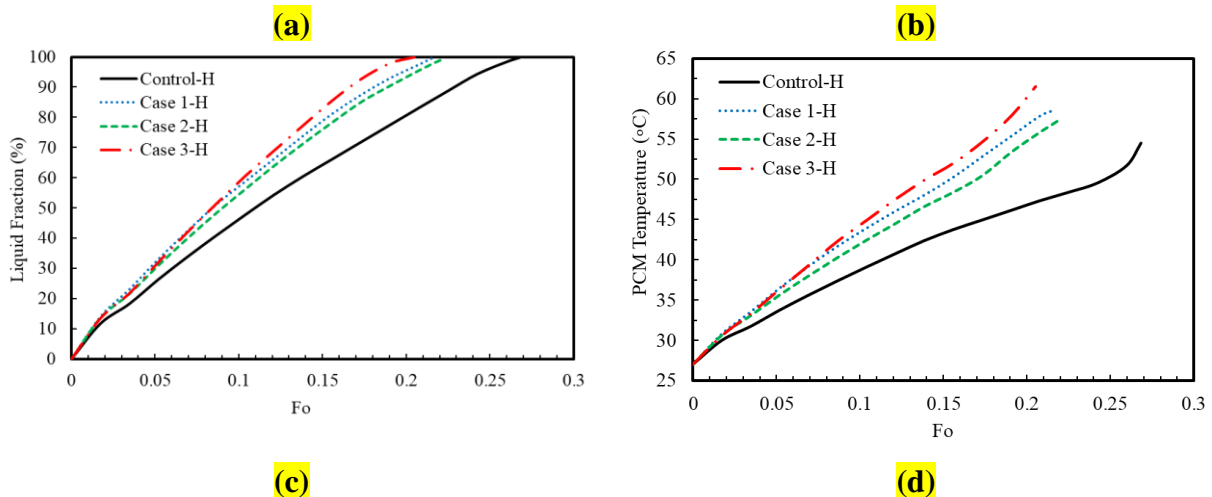
Fig. 5 reveals that using a small oscillator plate could enhance the melting rate (Fig. 5(a)) and improve the **absorbed heat energy rate** (Fig. 5(b)-(d)). Based on Fig. 5(a), using an oscillator may increase the melting process and reduce the complete melting time by 19.3%, 17.7%, and 23.6% with respect to control-H, for Case 1-H, Case 2-H, and Case 3-H, respectively. According to Fig. 5(a), Cases 1-H and 2-H have almost the same performance in melting rate enhancement, while Case 3-H shows a better condition for enhancing the melting rate. The reason may return to the oscillating direction in line with the gravity direction in Case 3-H. It could intensify the convective

heat transfer through mixing from the hot plate side to the solid-liquid interface of the PCM and vice versa due to its transversal oscillating direction compared to the longitudinal oscillating direction in Cases 1-H and 2-H, which plays a crucial role in heat transfer rate improvement as also reported in Ref. [34].

The average temperature of PCM during the charging process for each of Control-H, Cases 1-H, 2-H, and 3-H is shown in Fig. 5(b). Case 3-H has the highest temperature, followed by Case 1-H, 2-H, and Control-H. At a definite time, the higher PCM temperature between different cases means more heat absorption by that case. The heat transfer rate (Nusselt number) of the Control-H and these three cases have also been compared in Fig. 5(c) during the charging process. Fig. 5(c) indicates that using a small oscillator plate could enhance the Nusselt number from an average of 10.84 for the Control-H to 13.95 for Case 1-H (28.7% improvement), 13.85 for Case 2-H (27.7% improvement), and 15.04 for Case 3-H (38.7% improvement), respectively. Case 3-H has the highest heat transfer rate, especially after the liquid fraction exceeds 20%, which originated from causing transversal mixing flow from the hot plate to the solid-liquid interface, which is in line with gravity and intensifies the natural convection at the bottom of the heat sink. For the liquid fraction less than 20%, the oscillator vibration is damped by the solid PCM near the oscillator due to the oscillating direction. As a result, mixing heat flow was found to be minimum and could not affect the heat transfer rate. It has led to a small Nusselt number for Case 3-H at low liquid fractions. The heat transfer rate of Cases 1-H and 2-H is similar, especially for the liquid fraction less than 20% and when it exceeds 50% of the heat sink. While Case 1-H shows a higher Nusselt number for  $20% < \text{liquid fraction} < 50\%$ . Because the distance between the oscillator plate and solid-liquid interface in Case 1-H is lower for  $20% < \text{liquid fraction} < 50\%$  (it will be shown later in Fig. 8). Therefore, the mixing heat flow could be transferred more easily to the solid-liquid interface and helps to speed up the melting. As soon as the liquid fraction exceeds 50%, the average

distance between the oscillator plate and the solid-liquid interface for both Cases 1-H and 2-H becomes almost identical (it will be shown later in Fig. 8), as a result, the heat transfer rates (Nusselt number) of these two cases approached to each other.

To compare the performance of each horizontal thermal energy storage unit, the absorbed heat energy rate up to  $Fo = 0.2$ ,  $AHR(Fo=0.2)$ , has been calculated based on Eq. (16) and compared in Fig. 5(d). Also, the oscillating energy up to  $Fo = 0.2$  has been computed using Eq. (12) for Cases 1-H, 2H, and 3-H in Fig. 5(d). Fig. 5(d) reveals that although using an oscillator could improve the absorbed heat energy rate (AHR) from 0.58 for Control-H to 0.72 for Case 1-H (24.1% improvement), 0.71 for Case 2-H (22.4% improvement), and 0.76 for Case 3-H (31% improvement). So, Cases 1-H, 2-H, and 3-H could increase the absorbed heat by 3.17 kJ, 2.95 kJ, and 4.08 kJ, respectively. While the oscillating energy requires for each case is in magnitude order of mJ which is much lower than the thermal energy increment with kJ order of magnitude. The main superiority of the proposed small oscillator plate is the small oscillating energy demand in magnitude order of mJ which is considerably lower than that of the whole volumetric vibration of the thermal energy storage unit, which was presented in the literature [34,35] before. Due to the highest heat transfer rate (Nusselt number) in Case 3-H Fig. 5(c), the AHR experiences the maximum enhancement in Case 3-H by about 31% compared to Cases 1-H and 2-H.



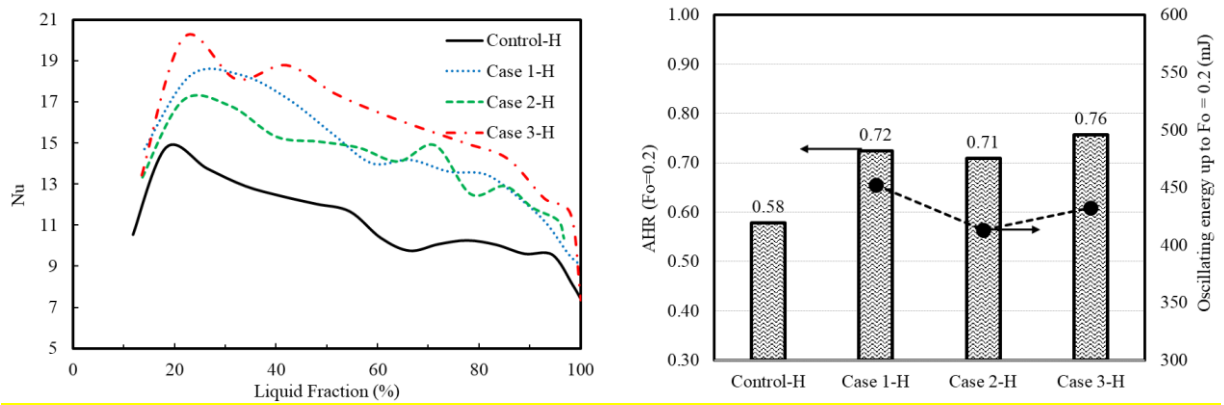


**Fig. 5.** Comparison of the (a) liquid fraction, (b) average temperature, (c) Nusselt number, and (d) absorbed heat energy rate and oscillating energy between the horizontal PCM thermal energy storage units including Control-H (without oscillator), Case 1-H, Case 2-H, and Case 3-H.

The vertically-oriented thermal energy storage units in Fig. 1 (Cases 1-V, 2-V, and 3-V) have also been evaluated in Fig. 6.

The reported results in Fig. 6 show that using an oscillator plate also has beneficial effects in decreasing the complete melting time, increasing the heat transfer rate, and augmenting the absorbed heat energy rate. Using the oscillator plate could reduce the complete melting time by 30%, 36%, and 39% for Cases 1-V, 2-V, and 3-V, respectively, compared to Control-V, see Fig. 6(a). Fig. 6(b) shows that Cases 1-V, 2V, and 3-V have a higher average temperature for a given time compared to Control-V, which means that these cases are more successful in intensifying the Nusselt number, as illustrated in Fig. 6(c), and also AHR, as indicated in Fig. 6(d).

According to Fig. 6, Cases 1-V and 2-V with the same oscillating direction show almost the same performance in the melting process, the heat transfer rate (Nu), and the absorbed heat energy rate (AHR). It reveals that the place of the oscillator plate is insignificant for vertically-oriented thermal energy storage when the oscillating direction is in line with the gravity direction. However, the heat transfer rate (Nusselt number) of Case 1-V begins to reduce more rapidly than Case 2-V when the liquid fraction exceeds 80%. It is because all the solid PCM, which is near the oscillator plate of Case 1-V, is going to be melted as soon as the liquid fraction exceeds 80%, so the solid-liquid

interface moves away from the oscillator plate and makes a considerable distance from the oscillator plate. This issue makes the role of the oscillator plate of Case 1-V in mixing heat flow and melting process less. While the oscillator plate of Case 2-V is still close to the solid-liquid interface even after the liquid fraction exceeds 80% and could play its improving role in producing mixing heat flow and intensifying the heat transfer rate in Fig. 6(c). Therefore, the melting rate, average PCM temperature, and heat transfer rate of Case 2-V are overtaken those of Case 1-V after the liquid fraction exceeded 80%. Of course, due to the slight superiority of Case 1-V over Case 2-V in the heat transfer rate for the liquid fraction less than 80%, as shown in Fig. 6(c), the AHR up  $Fo = 0.2$  in Case 1-V is a bit more than Case 2-V, see Fig. 6(d).

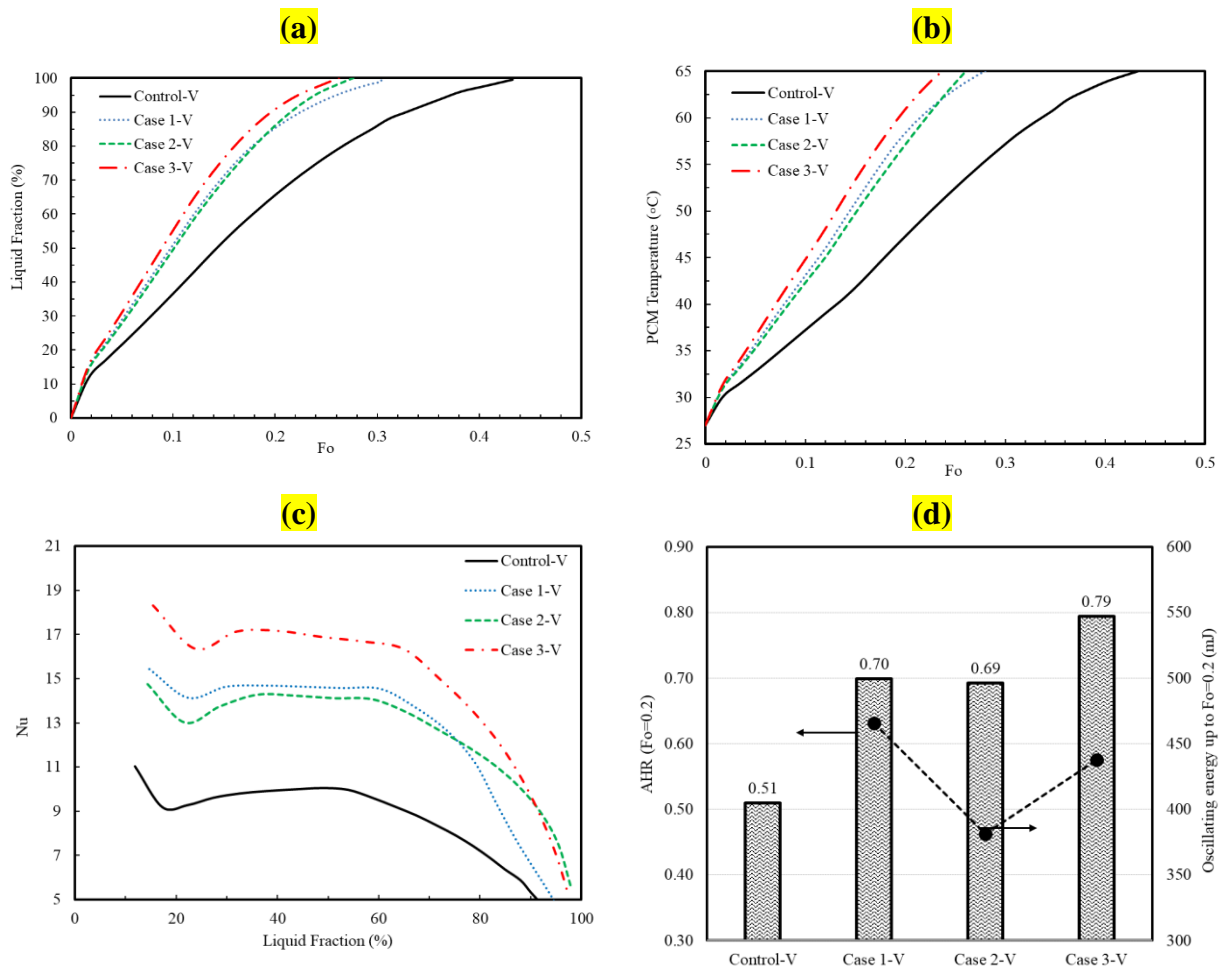


**Fig. 6.** Comparison of the (a) liquid fraction, (b) average temperature, (c) Nusselt number, and (d) absorbed heat energy rate and oscillating energy between the vertical PCM thermal energy storage units including Control-V (without oscillator), Case 1-V, Case 2-V, and Case 3-V.

The results of Fig. 6 demonstrate that the transversal oscillating direction of Case 3-V, which is perpendicular to the gravity direction and guides the mixing heat flow from the hot plate to the solid-liquid interface and vice versa has the fastest melting rate (see Fig. 6(a)), the highest Nusselt number (see Fig. 6(c)), and the maximum **AHR** (see Fig. 6(d)) in comparison to Cases 1-V and 2-V. The small oscillator plate in Case 3-V is placed at the left bottom of the PCM heat sink, which plays its crucial role in transferring the mixing heat flow to the solid PCM from the beginning to complete melting time; therefore, Case 3-V has the maximum heat transfer rate during all the melting time, see Fig. 6 (a)-(c). As a result, the average Nusselt number is enhanced from 8.28 for Control-V to 13.6 for Case 3-V (64.2% improvement), while it reaches 10.25 and 11.96 for Cases 1-V and 2-V, respectively, which shows 23.8% and 44.4% improvements, correspondingly. Fig. 6(d) also shows the superiority of Case 3-V in **absorbed heat energy rate**, which increases the **AHR** **from 0.51 for Control-V to 0.79 for Case 3-V (54.9% improvement)**. It is 0.7 and 0.69 for Cases 1-V and 2-V, respectively, with 37.2% and 35.3% improvements. On the other hand, based on Fig. 6(d), the oscillating energy required for each of the cases is, to some extent, equal and negligible compared to the enhancement of the **AHR**.

To investigate the power of the friction and drag force exerted on the oscillator plate, the profiles of velocity, friction drag force, and drag power have been calculated and plotted in Fig. 7 for Cases 3-H and 3-V, as examples, during a vibrating time period. The velocity profile, red curve plotted in Fig. 7, is the one that is expressed as boundary conditions to the oscillator plate in Eq. (9). The friction drag force exerted on the oscillator plate, green curve, which is calculated from the CFD simulation is exactly in the opposite direction of the velocity. Finally, the power of the drag force is obtainable by multiplying the drag force by the velocity as described before in Eq. (13); it is

plotted as the blue curve in Fig. 7. According to Fig. 7, the time period of drag power is reduced to half of the velocity time period. It is worthwhile to note that the required oscillating energy is computed by integrating the drag power over the time for all the melting times reported in Fig. 5(d) and Fig. 6(d). The low oscillating energy needed for the small oscillator plate is one superiority of the proposed design compared to the vibration of the whole volume of the PCM heat sink, which Refs. [34,36] have suggested. Here, the enclosed area of the drag power profile in Fig. 7, the blue curve, represents the required oscillating energy for one complete vibration cycle, which is 0.03 mJ for both Cases 3-H and 3-V, which is very low.

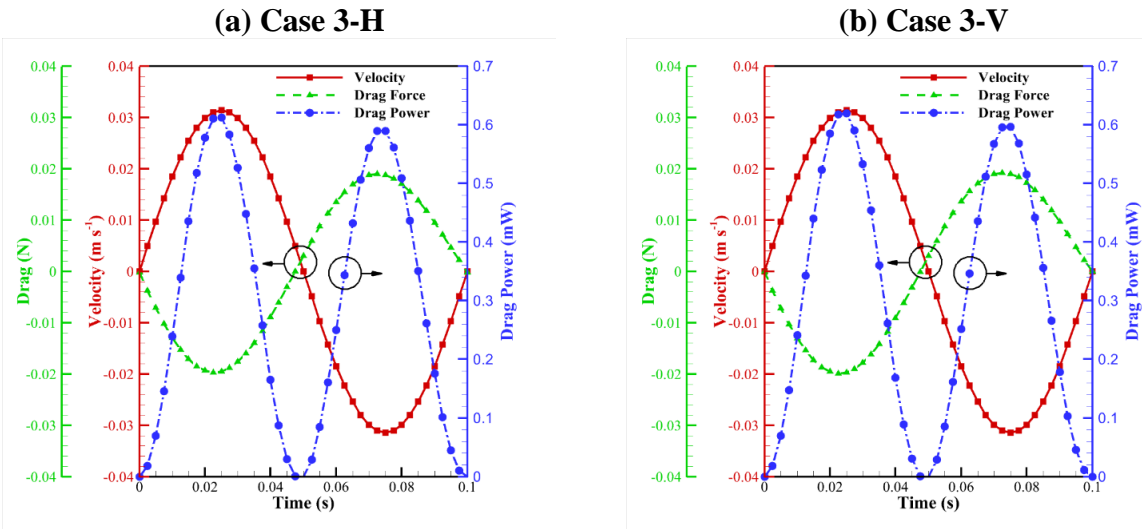


**Fig. 7.** The oscillator plate's velocity, force, and power profiles for (a) Case 3-H and (b) Case 3-V during a vibrating period.

The contour plots of the liquid fraction, temperature, vorticity, and streamlines have been illustrated for the horizontally- and vertically-oriented thermal energy storage units in Fig. 8 and Fig. 9, respectively. Comparing the liquid fraction contours in Fig. 8 and Fig. 9 reveals that using a small oscillator could increase the melting rate considerably compared to the Control cases with no oscillator plate. For the horizontal PCM heat sinks, Cases 1-H, 2-H, and 3-H, the oscillator plate makes a considerable mixing heat flow and, by using the buoyancy force, directs it to the solid-

liquid interface placed at the top region of the oscillator. This issue can be seen in the temperature contours in Fig. 8. Meanwhile, for the vertical PCM heat sink, Cases 1-V, 2-V, and 3-V, the mixing heat flow, which is induced by the oscillator plate is directed to the top of the heat sink by the buoyancy force and makes to melt the solid PCM located at the top region of the solid-liquid interface. This mixing heat flow does not considerably influence the melting of the solid-liquid interface facing the oscillator; this issue can be seen in the liquid fraction and temperature contours of Fig. 9.

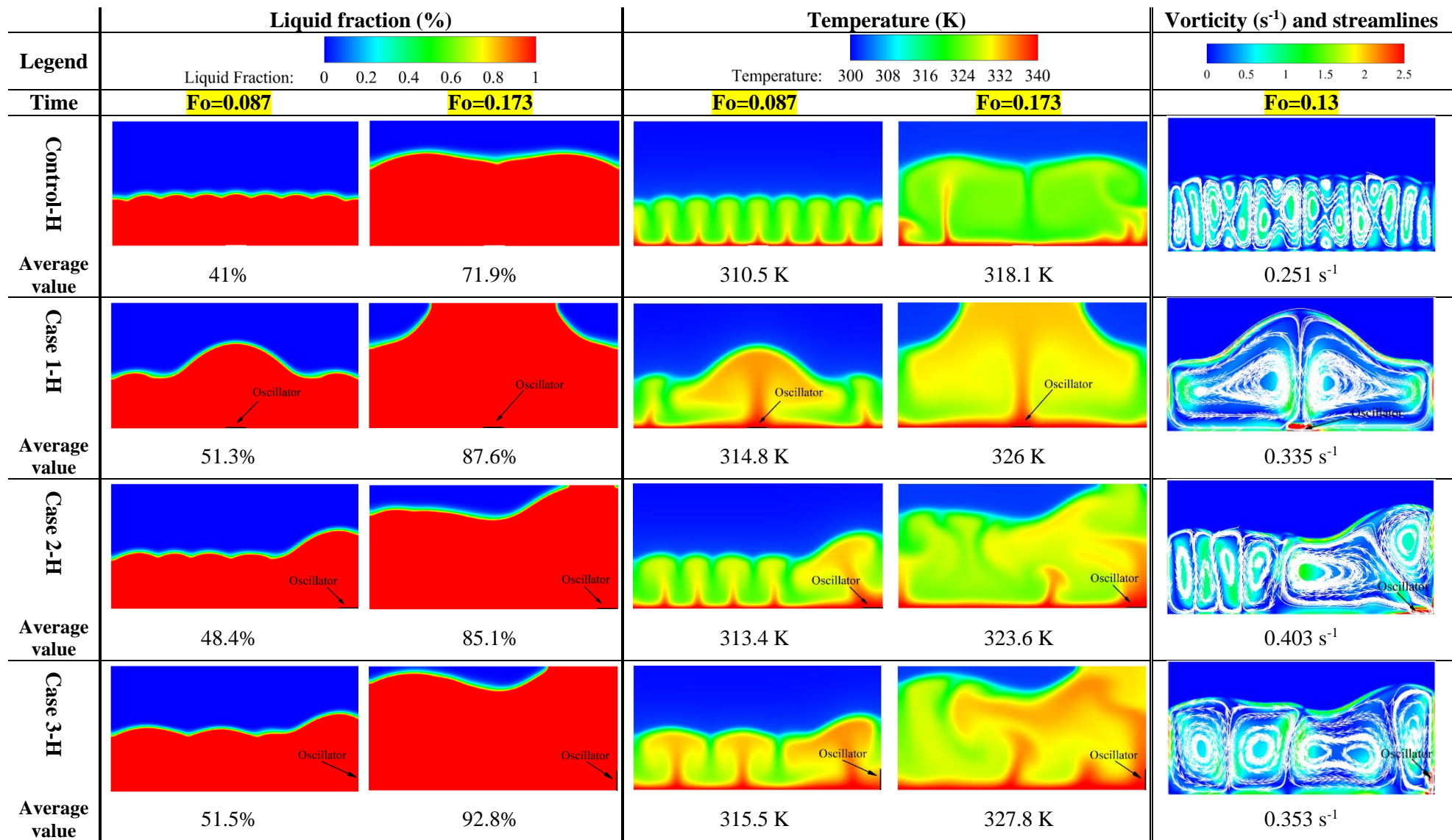


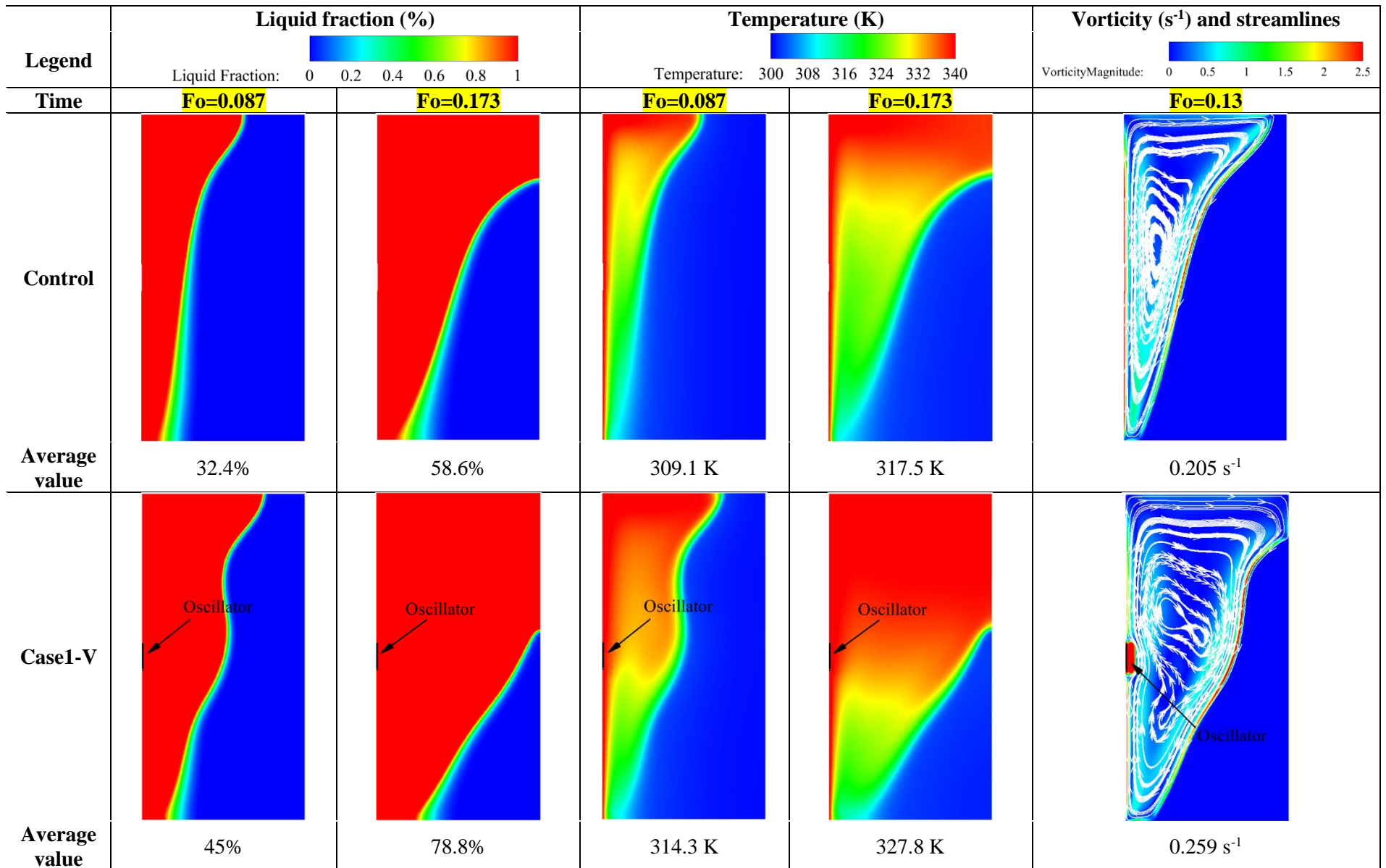
**Fig. 8.** Contour plots of liquid fraction, the temperature at **Fo=0.087** and **Fo=0.173**, and the vorticity and streamlines at **Fo=0.13** for Control-H, Case 1-H, Case 2-H, and Case 3-H.

0 To investigate the amount and manner of mixing heat convective flow in different PCM heat  
1 sinks, the contours of vorticity and streamlines are plotted for the horizontally- and vertically-  
2 oriented heat sinks in Fig. 8, and Fig. 9, respectively. As indicated in Fig. 8, when there is no  
3 oscillator plate, Control-H, many small convective vortexes tend to direct the convective heat to  
4 the solid-liquid interface to melt the solid PCM. However, when an oscillator plate is used, these  
5 small vortexes are organized and joined to form bigger, stronger vortexes in Cases 1-H, 2-H, and  
6 3-H. So that the average value of vorticity is enhanced from  $0.251 \text{ s}^{-1}$  for Control-H to  $0.335 \text{ s}^{-1}$   
7 for Case 1-H (33.5% enhancement),  $0.403 \text{ s}^{-1}$  for Case 2-H (60.5% enhancement), and  $0.353 \text{ s}^{-1}$   
8 for Case 3-H (40.6% enhancement) at  $\text{Fo} = 0.13$ , it demonstrates the positive effects of using an  
9 oscillator to enhance the natural heat convective flow. For vertically-oriented heat sinks, as shown  
10 in Fig. 9, the vortexes of the natural convective heat flow are large and integrated for the base  
11 case heat sink, Control-V, with no oscillator. However, using an oscillator could make some local  
12 vortexes near the oscillator, which intensify the average value of vorticity from  $0.205 \text{ s}^{-1}$  for  
13 Control-V to  $0.259 \text{ s}^{-1}$  for Case 1-V (26.3% enhancement),  $0.292 \text{ s}^{-1}$  for Case 2-V (42.4%  
14 enhancement), and  $0.288 \text{ s}^{-1}$  for Case 3-V (40.5% enhancement) at  $\text{Fo} = 0.13$ .  
15 As a result of Fig. 8 and Fig. 9, for both horizontally- and vertically-oriented heat sinks, using a  
16 small oscillator plate in Cases 1, 2, and 3, respectively, leads to greater enhancement in the  
17 melting and heat transfer rates.

18

19

20



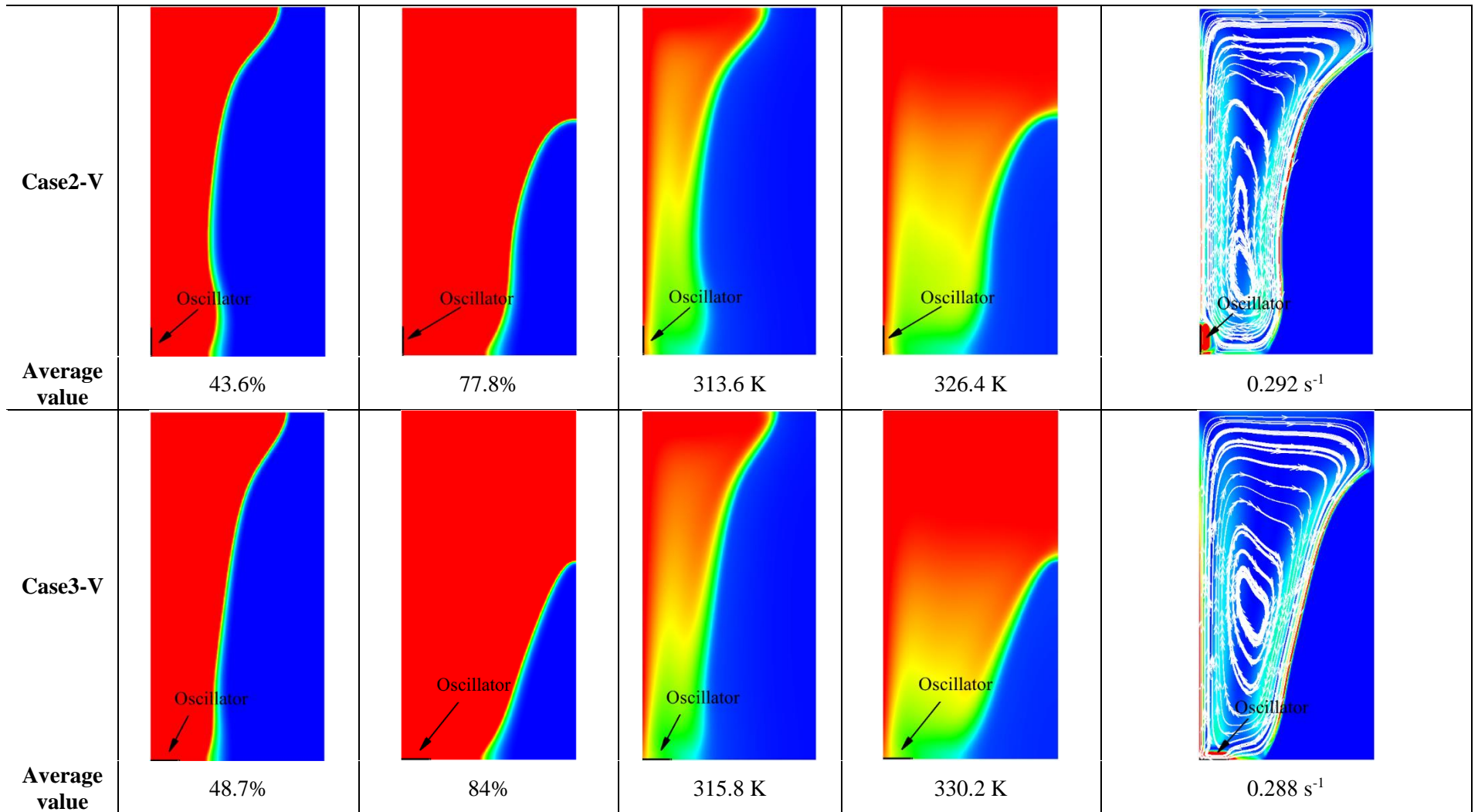


**Fig. 9.** Contour plots of liquid fraction, the temperature  $Fo=0.087$  and  $Fo=0.173$ , and the streamline and vorticity at  $Fo=0.13$  for Control-V, Case 1-V, Case 2-V, and Case 3-V.

22 Here, the effect of oscillating amplitude as one of the most significant vibration parameters has  
23 been studied and reported in Fig. 10. The vertical PCM heat sinks are considered to investigate the  
24 effect of changing oscillating amplitude from  $V_a = 0.01\pi$  ( $\text{m s}^{-1}$ ) (in Eq. (9)) to  $5V_a$ . Based on Fig.  
25 10, changing oscillating amplitude has a little, significant, and very slight effect on the time profile  
26 of the liquid fraction for Cases 1-V, 2-V, and 3-V, respectively. Increasing the oscillating  
27 amplitude from  $V_a$  to  $5V_a$  does not help to improve the heat transfer in Cases 1-V and 3-V  
28 considerably. Because the oscillator is placed in the middle of the hot plate in Case 1-V, so  
29 increasing the oscillating amplitude leads to rising the mixing flow at the top region of the heat  
30 sink, which is the hottest place with an inherent considerable potential for free natural convective  
31 due to the buoyancy force. Thus, increasing the oscillating amplitude does not lead to much further  
32 improvement in Case 1-V. On the other hand, the oscillator of Case 3-V is located at the bottom  
33 left of the heat sink, which is close to the solid-liquid interface through the melting time. It means  
34 that increasing the oscillating amplitude will usually be damped by the solid PCM and does not  
35 have a considerable effect. However, Case 2-V could benefit from increasing the oscillating  
36 amplitude due to the proper oscillator position. In fact, increasing the oscillating amplitude raises  
37 the mixing heat flow domain along the heat sink and enhances the melting rate. So, for Case 2-V,  
38 the complete melting time reduces from  $\text{Fo} = 0.303$  for the oscillating amplitude of  $V_a$  to  $\text{Fo} =$   
39  $0.237$  for the oscillating amplitude of  $5V_a$  (21.9% reduction); see Fig. 10(b). Therefore, as shown  
40 in Fig. 10(d), Case 2-V has the highest **AHR** improvement of 6.56% by increasing the oscillating  
41 amplitude from  $V_a$  to  $5V_a$ , and then followed by Case 1-V with 4.11% and Case 3-V with 1.98%  
42 improvement, respectively. In conclusion to this fact, the position of the oscillator plate is  
43 significant in determining the optimum oscillating amplitude.

44

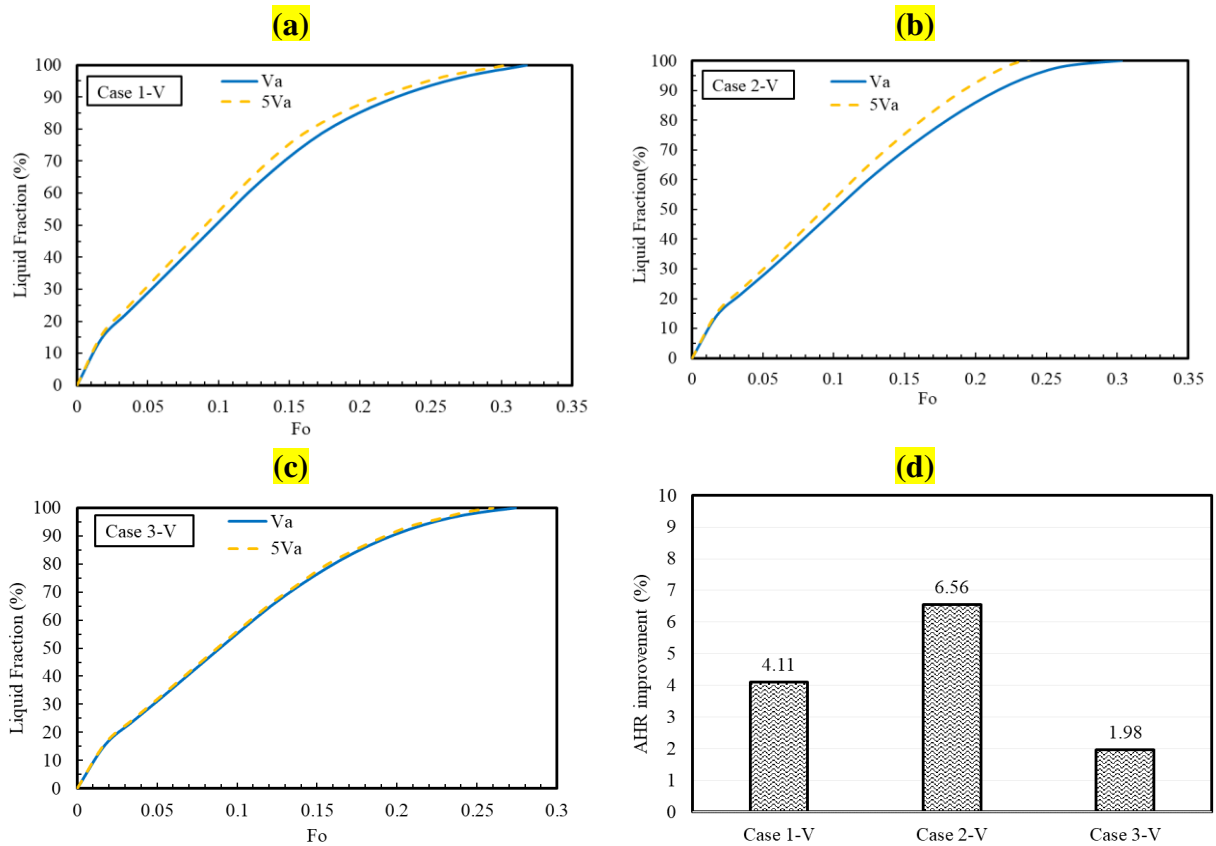


**Fig. 10.** Influence of the oscillation amplitude on the liquid fraction of PCM heat sinks (a) Case 1-V, (b) Case 2-V, (c) Case 3-V, and on (d) absorbed heat energy rate (AHR) improvement.

45

46 Finally, to have a complete evaluation of all the horizontally- and vertically-oriented PCM heat  
 47 sinks studied here, the averaged Nusselt number and the AHR are computed and compared in Fig.  
 48 11. Fig. 11 shows that both the averaged Nusselt number and the AHR have been enhanced for  
 49 Cases 1, 2, and 3 in both horizontal and vertical orientations compared to its Control case. It proves  
 50 that using an oscillator positively influences the mixing heat flow within the PCM heat sink,  
 51 improving the heat transfer rate. Comparing the horizontal and vertical orientation in Fig. 11, one  
 52 can say that the averaged Nusselt number (heat transfer rate) in the horizontal cases is more than  
 53 the vertical ones. The reason returns to the inclination angle of the PCM heat sink, which depends  
 54 on the orientation of the hot plate, so that the bigger the inclination angle (which means the hot  
 55 plate at the bottom = horizontally-oriented heat sinks), the higher the natural convective heat flow.

56 According to Fig. 11, both Cases 3-H and 3-V have the maximum Nusselt number (15.04 for Case  
 57 3-H and 13.60 for Case 3-V), which yields the maximum net **AHR (0.76 for Case 3-H and 0.79**  
 58 **for Case 3-V)**. It reveals that transversal oscillating, which occurs in Cases 3-H and 3-V is more  
 59 effective in directing the mixing heat flow to the solid-liquid interface in order to accelerate the  
 60 melting process. While the longitudinal oscillating (compared to transversal), which occurs in  
 61 Cases 1-H, 2-H, 1-V, and 2-V, is less helpful in this regard. Fig. 11 also shows the improvements  
 62 in the Nusselt number and **AHR** experienced by Cases 1, 2, and 3 compared to the Control case.  
 63 Based on Fig. 11, using an oscillator plate leads to a higher improvement of the Nusselt number  
 64 and **AHR** in vertically-oriented PCM heat sinks compared to the horizontally-oriented ones. This  
 65 issue reflects that the vertical heat sinks, which have a weaker inherent natural convective rate,  
 66 benefit more from oscillator plates than the horizontal ones.

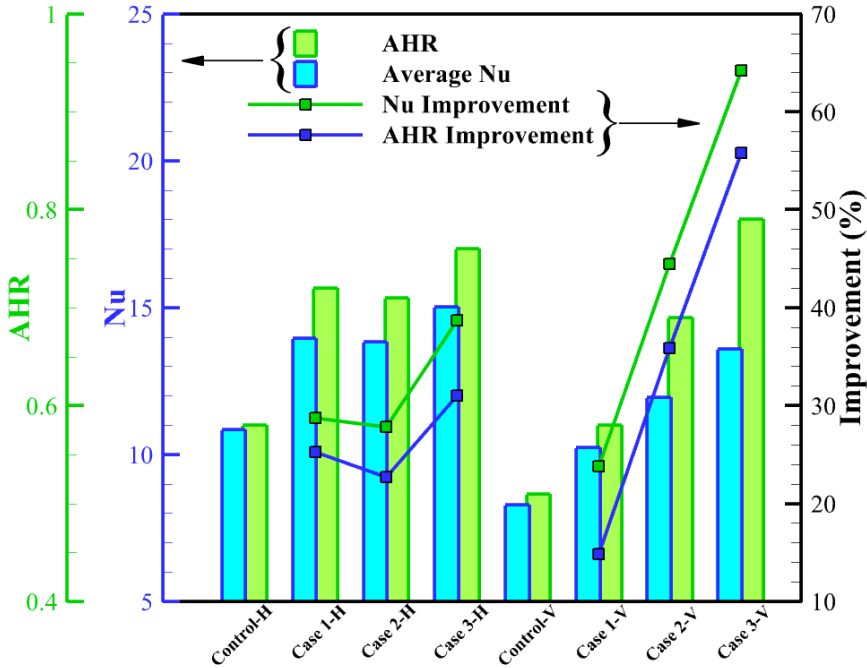


**Fig. 11.** Comparison of the Nusselt number and the absorbed heat energy rate (AHR) between the horizontally- and vertically-oriented PCM heat sinks. Bars represent the Nusselt number and AHR and are read from the left axis, and lines with markers represent the improvement in the Nusselt number and the AHR with respect to the Control case and are read from the right axis.

#### 67 4. Concluding Remarks

68 Current research suggests using a small oscillator plate to enhance the performance of thermal  
69 energy storage units by making mixing heat flow and directing it to the solid-liquid interface to  
70 hasten the melting process. The influence of using an oscillator plate within three different  
71 configurations for both horizontally- and vertically-oriented PCM heat sinks, including i)  
72 longitudinal oscillating at the middle of the hot plate (named as Cases 1-H, and 1-V for horizontal  
73 and vertical heat sinks, respectively), ii) longitudinal oscillating at the corner of the hot plate  
74 (named as Cases 2-H, and 2-V for horizontal and vertical heat sinks, respectively), and iii)  
75 transversal oscillating at the corner of the heat sink (named as Cases 3-H, and 3-V for horizontal  
76 and vertical heat sinks, respectively). A complete computational fluid dynamics model has been  
77 employed to model the heat transfer and PCM melting process and evaluate the induced mixing  
78 heat flow and its effect on natural convection. Due to the lack of results for a small oscillator plate,  
79 the present model has been validated against the results of a PCM thermal energy storage unit with  
80 a full volumetric oscillator. The model is also evaluated as mesh grid size and time step  
81 independent. The effect of oscillator amplitude is also investigated. The most significant results of  
82 the present study, which help enhance the performance of thermal energy storage units and develop  
83 their application, are reported as follows:

- 84 • Using a small oscillator plate leads to directing the mixing heat flow to the solid-liquid  
85 interface. It hastens the melting process by 19.3%, 17.7%, and 23.6% for Cases 1-H, 2-H,  
86 and 3-H, respectively, compared to Control-H (without oscillator) and 30%, 36%, and 39%  
87 for Cases 1-V, 2-V, and 3-V, respectively, compared to Control-V (without oscillator).
- 88 • Nusselt number has been improved from an average of 10.84 for the Control-H to 13.95  
89 for Case 1-H (28.7% improvement), 13.85 for Case 2-H (27.7% improvement), and 15.04  
90 for Case 3-H (38.7% improvement), respectively. Also, the average Nusselt number is

91 enhanced from 8.28 for Control-V to 13.6 for Case 3-V (64.2% improvement), while it  
92 reaches 10.25 and 11.96 for Cases 1-V and 2-V, respectively, which shows 23.8% and  
93 44.4% improvements, correspondingly.

94 • Transversal oscillating, which occurs in Cases 3-H and 3-V, is more effective in directing  
95 the mixing heat flow to the solid-liquid interface in order to accelerate the melting process.

96 • An oscillator could improve the AHR from 0.58 for Control-H to 0.72 for Case 1-H (24.1%  
97 improvement), 0.71 for Case 2-H (22.4% improvement), and 0.76 for Case 3-H (31%  
98 improvement). Meanwhile, the AHR increases from 0.51 for Control-V to 0.7, 0.69, and  
99 0.79 for Cases 1-V, 2-V, and 3-V, respectively, corresponding to 37.2%, 35.3%, and 54.9%  
100 improvement.

101 • Although the PCM heat sinks, which are equipped with oscillator plates, could absorb  
102 considerably more heat in the range of 2.95-4.08 kJ and 4.13-6.43 kJ for the horizontally-  
103 and vertically-oriented heat sinks, respectively, the oscillating energy required for each  
104 case is in magnitude order of 413-452 mJ and 380-465 mJ for the horizontally- and  
105 vertically-oriented heat sinks, respectively which are much lower than the thermal energy  
106 increment. While oscillating energy requires the full volumetric vibration of the PCM heat  
107 sink suggested in the literature, Refs. [34,36], is considerable.

108 • Using an oscillator plate leads to a higher improvement of the Nusselt number and AHR  
109 in vertically-oriented PCM heat sinks than the horizontally-oriented ones.

110 Novel findings of the recent study seem useful to extend the technology of PCM thermal energy  
111 storage units and expand its application worldwide.

112

113

114

115 **Credit author statement**

116 **S. Rahmanian:** Supervision, Conceptualization, Investigation, Methodology, Experimental  
117 efforts, Reviewing and editing, Writing-Original draft preparation. **H. Rahmanian-Koushkaki:**  
118 Conceptualization, Investigation, Experimental efforts, Writing-Original draft preparation,  
119 Reviewing, and editing. **M. Moein-Jahromi:** Conceptualization, Investigation, Methodology,  
120 Experimental efforts, Visualization, Data curation, Results post-processing, Writing-Original draft  
121 preparation. **R. Saidur:** Conceptualization, Investigation, Reviewing and editing.

122 **Declaration of Competing Interest**

123 The authors declare that they have no known competing financial interests or personal  
124 relationships that could have appeared to influence the work reported in this paper.

125 **Acknowledgments**

126 This research did not receive any specific grant from funding agencies in the public, commercial,  
127 or not-for-profit sectors.

## Nomenclature

### Symbols

$A_{mush}$	Mushy zone constant [ $\text{kg m}^{-3} \text{s}^{-1}$ ]
$C_p$	Specific heat [ $\text{J kg}^{-1} \text{K}^{-1}$ ]
$D$	Depth of heat sink [m]
$E_{mech}$	Mechanical energy [J]
$E_{heat}$	Total absorbed heat energy [J]
$f$	Frequency (Hz)
$g$	Gravitational acceleration [ $9.81 \text{ m s}^{-2}$ ]
$H$	Total enthalpy [ $\text{J kg}^{-1}$ ]
$h$	Heat transfer coefficient [ $\text{W m}^{-2} \text{K}^{-1}$ ]
$h_{sl}$	Latent heat of fusion for the PCM [ $\text{J kg}^{-1}$ ]
$k$	Thermal conductivity [ $\text{W m}^{-1} \text{K}^{-1}$ ]
$L$	Length of heat sink [m]
$L_f$	Liquid fraction of the PCM [dimensionless]
$Nu$	Nusselt number [Dimensionless]
$P$	Pressure [Pa]
$P_d$	Mechanical power which is needed to overcome the friction drag force [W]
$q''$	Heat flux [ $\text{W m}^{-2}$ ]
$S$	Source term [ $\text{kg m}^{-2} \text{s}^{-2}$ ]
$t$	Time (s)
$T$	Temperature [K]
$u$	x velocity component [ $\text{m s}^{-1}$ ]
$v$	y velocity component [ $\text{m s}^{-1}$ ]
$\vec{V}$	Velocity vector [ $\text{m s}^{-1}$ ]
$V_a$	Amplitude of the oscillating velocity function [ $\text{m s}^{-1}$ ]
$V_p$	Velocity of oscillator plate [ $\text{m s}^{-1}$ ]
$W$	Width of thermal energy storage unit [m]

### Greek letters

$\beta$	Thermal expansion coefficient [ $\text{K}^{-1}$ ]
$\eta_{elec}$	Efficiency [Dimensionless]
$\epsilon$	Numerical constant [0.001]
$\mu$	Viscosity [Pa s]
$\rho$	Density [ $\text{kg m}^{-3}$ ]
$\tau_w$	Wall shear stress [Pa]

### Subscribes

l	Liquid
pcm	Phase change material
s	Solid
p	Plate

### Abbreviations

CFD	Computational fluid dynamics
FVM	Finite volume method
PCM	Phase change material

LHS	Latent heat storage
TES	Thermal energy storage

## Figures Captions:

**Fig. 1.** Schematic view of the thermal energy storage units equipped with an oscillator plate, (a) to (c) are horizontally oriented, and (d) to (f) are vertically oriented PCM containers.

**Fig. 2.** Sample of solution domain with the mesh grids for Case 1-H. Red line: hot plate, blue lines: adiabatic boundaries, black line: oscillator plate.

**Fig. 3.** Validation of the present simulation against the numerical modeling of Wu et al. [34], (a) liquid fraction, and (b) Nusselt number for frequency of 0.0002 Hz.

**Fig. 4.** Solution independency study with respect to (a) grid size and (b) time step for Case 3-H.

**Fig. 5.** Comparison of the (a) liquid fraction, (b) average temperature, (c) Nusselt number, and (d) absorbed heat energy rate and oscillating energy between the horizontal PCM thermal energy storage units including Control-H (without oscillator), Case 1-H, Case 2-H, and Case 3-H.

**Fig. 6.** Comparison of the (a) liquid fraction, (b) average temperature, (c) Nusselt number, and (d) absorbed heat energy rate and oscillating energy between the vertical PCM thermal energy storage units including Control-V (without oscillator), Case 1-V, Case 2-V, and Case 3-V.

**Fig. 7.** The oscillator plate's velocity, force, and power profiles for (a) Case 3-H and (b) Case 3-V during a vibrating period.

**Fig. 8.** Contour plots of liquid fraction, the temperature at  $Fo=0.087$  and  $Fo=0.173$ , and the vorticity and streamlines at  $Fo=0.13$  for Control-H, Case 1-H, Case 2-H, and Case 3-H.

**Fig. 9.** Contour plots of liquid fraction, the temperature  $Fo=0.087$  and  $Fo=0.173$ , and the streamline and vorticity at  $Fo=0.13$  for Control-V, Case 1-V, Case 2-V, and Case 3-V.

**Fig. 10.** Influence of the oscillation amplitude on the liquid fraction of PCM heat sinks (a) Case 1-V, (b) Case 2-V, (c) Case 3-V, and on (d) absorbed heat energy rate (AHR) improvement.

**Fig. 11.** Comparison of the Nusselt number and the absorbed heat energy rate (AHR) between the horizontally- and vertically-oriented PCM heat sinks.

**Tables Captions:**

**Table 1.** Thermo-physical properties of materials used in this study [31] and for validation [34].

## References

- [1] Zhang J, Cao Z, Huang S, Huang X, Han Y, Wen C, et al. Solidification performance improvement of phase change materials for latent heat thermal energy storage using novel branch-structured fins and nanoparticles. *Appl Energy* 2023;342:121158. <https://doi.org/https://doi.org/10.1016/j.apenergy.2023.121158>.
- [2] Luo J, Gu H, Wang S, Wang H, Zou D. A coupled power battery cooling system based on phase change material and its influencing factors. *Appl Energy* 2022;326:119917. <https://doi.org/https://doi.org/10.1016/j.apenergy.2022.119917>.
- [3] Heyhat MM, Mousavi S, Siavashi M. Battery thermal management with thermal energy storage composites of PCM, metal foam, fin and nanoparticle. *J Energy Storage* 2020;28:101235. <https://doi.org/10.1016/j.est.2020.101235>.
- [4] Kabbara M, Kheirabadi AC, Groulx D. Numerical modelling of natural convection driven melting for an inclined/finned rectangular enclosure. *ASME 2016 Heat Transfer Summer Conference, HT 2016, collocated with the ASME 2016 Fluids Engineering Division Summer Meeting and the ASME 2016 14th International Conference on Nanochannels, Microchannels, and Minichannels, vol. 2, 2016*. <https://doi.org/10.1115/HT2016-7068>.
- [5] Rahmanian S, Moein-Jahromi M, Rahmanian-Koushkaki H, Sopian K. Performance investigation of inclined CPV system with composites of PCM, metal foam and nanoparticles. *Solar Energy* 2021;230:883–901. <https://doi.org/10.1016/j.solener.2021.10.088>.
- [6] Rahmanian-Koushkaki H, Rahmanian S, Moein-Jahromi M, Sopian K. Performance evaluation of concentrated photovoltaics with phase change materials embedded metal foam-based heat sink using gradient strategy. *Int J Energy Res* 2022;46:12290–315. <https://doi.org/10.1002/er.7996>.
- [7] Moein-Jahromi M, Rahmanian-Koushkaki H, Rahmanian S, Jahromi SP. Evaluation of nanostructured GNP and CuO compositions in PCM-based heat sinks for photovoltaic systems. *J Energy Storage* 2022;53:105240.
- [8] Eslami M, Khosravi F, Fallah Kohan HR. Effects of fin parameters on performance of latent heat thermal energy storage systems: A comprehensive review. *Sustainable Energy Technologies and Assessments* 2021;47:101449. <https://doi.org/https://doi.org/10.1016/j.seta.2021.101449>.
- [9] Zhang S, Mancin S, Pu L. A review and prospective of fin design to improve heat transfer performance of latent thermal energy storage. *J Energy Storage* 2023;62:106825. <https://doi.org/https://doi.org/10.1016/j.est.2023.106825>.

- [10] Ghalambaz M, Jin H, Bagheri A, Younis O, Wen D. Convective Flow and Heat Transfer of Nano-Encapsulated Phase Change Material (NEPCM) Dispersions along a Vertical Surface. *Facta Universitatis, Series: Mechanical Engineering* 2022;20:519–38.
- [11] Li C, Wu X, Li S, Yang W, Wu S, Liu X, et al. Research on the high thermal conductivity composite phase change materials with graphite nanosheets for battery thermal safety. *J Energy Storage* 2023;61:106718. <https://doi.org/https://doi.org/10.1016/j.est.2023.106718>.
- [12] Nie C, Deng S, Liu J, Rao Z. Performance evaluation of shell-tube latent heat storage unit using nanoparticles with cascaded concentration. *J Energy Storage* 2023;62:106892. <https://doi.org/https://doi.org/10.1016/j.est.2023.106892>.
- [13] Kittusamy RK, Rajagopal V, Felix PG. Numerical and experimental investigation on the melting heat transfer of nanographene-enhanced phase change material composites for thermal energy storage applications. *Int J Heat Mass Transf* 2023;206:123940. <https://doi.org/https://doi.org/10.1016/j.ijheatmasstransfer.2023.123940>.
- [14] Shirbani M, Siavashi M, Hosseini M, Bidabadi M. Improved thermal energy storage with metal foam enhanced phase change materials considering various pore arrangements: A pore-scale parallel lattice Boltzmann solution. *J Energy Storage* 2022;52:104744. <https://doi.org/https://doi.org/10.1016/j.est.2022.104744>.
- [15] Zhao Y, Zou B, Ding J, Ding Y. Experimental and numerical investigation of a hybrid battery thermal management system based on copper foam-paraffin composite phase change material and liquid cooling. *Appl Therm Eng* 2023;218:119312. <https://doi.org/https://doi.org/10.1016/j.applthermaleng.2022.119312>.
- [16] Zhang S, Yao Y, Jin Y, Shang Z, Yan Y. Heat transfer characteristics of ceramic foam/molten salt composite phase change material (CPCM) for medium-temperature thermal energy storage. *Int J Heat Mass Transf* 2022;196:123262. <https://doi.org/https://doi.org/10.1016/j.ijheatmasstransfer.2022.123262>.
- [17] Bouguila M, Samet A, Souf MA Ben, Hami A El, Haddar M. Thermal performances of finned heat sink filled with nano-enhanced phase change materials: Design optimization and parametric study. *Int J Heat Mass Transf* 2023;202:123710. <https://doi.org/https://doi.org/10.1016/j.ijheatmasstransfer.2022.123710>.
- [18] Zhuang Y, Li H, Xu W, Huang S-M. Experimental study on the melting performance of magnetic NEPCMs embedded in metal foam subjected to a non-uniform magnetic field. *Solar Energy Materials and Solar Cells* 2023;250:112077. <https://doi.org/https://doi.org/10.1016/j.solmat.2022.112077>.

- [19] Bianco N, Busiello S, Iasiello M, Mauro GM. Finned heat sinks with phase change materials and metal foams: Pareto optimization to address cost and operation time. *Appl Therm Eng* 2021;197:117436. <https://doi.org/https://doi.org/10.1016/j.applthermaleng.2021.117436>.
- [20] Izadi M, Sheremet M, Hajjar A, Galal AM, Mahariq I, Jarad F, et al. Numerical investigation of magneto-thermal-convection impact on phase change phenomenon of Nano-PCM within a hexagonal shaped thermal energy storage. *Appl Therm Eng* 2023;223:119984. <https://doi.org/https://doi.org/10.1016/j.applthermaleng.2023.119984>.
- [21] Cui W, Li X, Li X, Lu L, Ma T, Wang Q. Combined effects of nanoparticles and ultrasonic field on thermal energy storage performance of phase change materials with metal foam. *Appl Energy* 2022;309:118465.
- [22] Zhang N, Du Y. Ultrasonic enhancement on heat transfer of palmitic-stearic acid as PCM in unit by experimental study. *Sustain Cities Soc* 2018;43:532–7. <https://doi.org/https://doi.org/10.1016/j.scs.2018.08.040>.
- [23] Zhang W, Li X, Wu W, Huang J. Influence of mechanical vibration on composite phase change material based thermal management system for lithium-ion battery. *J Energy Storage* 2022;54:105237. <https://doi.org/https://doi.org/10.1016/j.est.2022.105237>.
- [24] Du W, Chen S. Effect of mechanical vibration on phase change material based thermal management module of a lithium-ion battery at high ambient temperature. *J Energy Storage* 2023;59:106465. <https://doi.org/https://doi.org/10.1016/j.est.2022.106465>.
- [25] Zeng S, Chen S, Wu G. Effect of inclination angle on melting process of phase change materials in a square cavity under mechanical vibration. *J Energy Storage* 2021;36:102392. <https://doi.org/https://doi.org/10.1016/j.est.2021.102392>.
- [26] Wu G, Chen S, Zeng S. Effects of mechanical vibration on melting behaviour of phase change material during charging process. *Appl Therm Eng* 2021;192:116914. <https://doi.org/https://doi.org/10.1016/j.applthermaleng.2021.116914>.
- [27] Yu Y, Chen S. Utilize mechanical vibration energy for fast thermal responsive PCMs-based energy storage systems: Prototype research by numerical simulation. *Renew Energy* 2022;187:974–86. <https://doi.org/https://doi.org/10.1016/j.renene.2022.02.010>.
- [28] Brent AD, Voller VR, Reid KTJ. Enthalpy-porosity technique for modeling convection-diffusion phase change: application to the melting of a pure metal. *Numeri Heat Transf A Appl* 1988;13:297–318.
- [29] Ghalambaz M, Aljaghtham M, Chamkha AJ, Abdullah A, Alshehri A, Ghalambaz M. Anisotropic metal foam design for improved latent heat thermal energy storage in a tilted enclosure. *Int J Mech Sci* 2023;238:107830. <https://doi.org/https://doi.org/10.1016/j.ijmecsci.2022.107830>.

- [30] Ghalambaz M, Hashem Zadeh SM, Mehryan SAM, Pop I, Wen D. Analysis of melting behavior of PCMs in a cavity subject to a non-uniform magnetic field using a moving grid technique. *Appl Math Model* 2020;77:1936–53. <https://doi.org/https://doi.org/10.1016/j.apm.2019.09.015>.
- [31] Esapour M, Hamzehnezhad A, Rabienataj Darzi AA, Jourabian M. Melting and solidification of PCM embedded in porous metal foam in horizontal multi-tube heat storage system. *Energy Convers Manag* 2018;171:398–410. <https://doi.org/10.1016/j.enconman.2018.05.086>.
- [32] Rahmanian S, Moein-Jahromi M, Rahmanian-Koushkaki H, Sopian K. Performance investigation of inclined CPV system with composites of PCM, metal foam and nanoparticles. *Solar Energy* 2021;230:883–901. <https://doi.org/10.1016/j.solener.2021.10.088>.
- [33] Rahmanian S, Rahmanian Koushkaki H, Shahsavar A. Numerical assessment on the hydrothermal behaviour and entropy generation characteristics of boehmite alumina nanofluid flow through a concentrating photovoltaic/thermal system considering various shapes for nanoparticle. *Sustainable Energy Technologies and Assessments* 2022;52:102143. <https://doi.org/https://doi.org/10.1016/j.seta.2022.102143>.
- [34] Wu G, Chen S, Zeng S. Effects of mechanical vibration on melting behaviour of phase change material during charging process. *Appl Therm Eng* 2021;192:116914. <https://doi.org/https://doi.org/10.1016/j.applthermaleng.2021.116914>.
- [35] Du W, Chen S. Effect of mechanical vibration on phase change material based thermal management module of a lithium-ion battery at high ambient temperature. *J Energy Storage* 2023;59:106465. <https://doi.org/https://doi.org/10.1016/j.est.2022.106465>.
- [36] Zeng S, Chen S, Wu G. Effect of inclination angle on melting process of phase change materials in a square cavity under mechanical vibration. *J Energy Storage* 2021;36:102392. <https://doi.org/https://doi.org/10.1016/j.est.2021.102392>.